J. Fluid Mech. (1972), *vol.* 53, *part* 2, *pp.* 227–255
Printed in Great Britain

The flow and stability of thin liquid films on a rotating disk

By A. F. CHARWAT, R. E. KELLY
School of Engineering and Applied Science, University of California, Los Angeles
AND C. GAZLEY
The RAND Corporation, Santa Monica, California

(Received 7 December 1970 and in revised form 9 November 1971)

Measurements of the thickness and the stability of thin films of liquid (1–150 μm thick) formed on a rotating horizontal disk are presented and correlated in terms of an asymptotic-expansion solution of the thin-film equations. Water, various alcohols and water with wetting activities were used to cover a range of viscosity (1–2·5 cP) and surface tension (20–72 dynes/cm). Smooth flow was found to occur in a region defined by the flow rate, rotational speed and physical properties of the liquid. Outside this region various wave patterns were observed (concentric, spiral and irregular waves). A linear theory of the stability of the film based on an extension of classical stability theories for plane films on inclined planes is given and contrasted with the experimental results. Surface phenomena associated with the use of wetting agents were found to have a strong effect on the stability of the film.

1. Introduction

Most of the theoretical and experimental research on the flow of a liquid in thin films deals with films formed under the action of gravity on stationary, inclined and vertical planes (e.g. Fulford 1964). Such films are of interest in connexion with the transfer of heat and the diffusion of mass across the liquid interface because a thin film presents a very large transfer surface for the volume of through-flow.

Very little information on films driven by centrifugal forces on rotating surfaces is available. Centrifugal forces can be much larger than gravity. The film on rotating disks can thus be made thinner more rapidly and the size of the equipment for a given through-flow can be made smaller than in the case of a film developing on a stationary inclined plane. This makes it attractive for certain applications. A certain amount of research on rotating films was done from the standpoint of the atomization of the liquid and is more concerned with how the film leaves the spinning surface than with the development of the film itself. Dorfman (1967) published a numerical solution of the thin-film equations on a spinning disk for the initial phases of its development. Espig & Hoyle (1965)

provided experimental measurements of the maximum film thickness and discussed briefly the waves formed on the surface. Some preliminary design reports aimed at various applications are available (water desalinization (Bromley 1965), oxygen transfer to blood (Aroesty *et al.* 1967; and others)). However, all this information is insufficient to predict the characteristics of a film of liquid with arbitrary physical properties (viscosity and surface tension) and the nature of the waves on the free surface of the film, which are important in determining the coefficients of heat and mass transfer across the interface.

Some preliminary results of the present programme have already been presented at scientific meetings. Aroesty *et al.* (1967) presented an asymptotic theory for the development of the film on a rotating disk. Measurements of the mean thickness of the film were discussed by Gazley & Charwat (1968). These experiments did not include variations in the properties of the liquid. The present paper summarizes the previous results and describes additional studies dealing with the stability of the surface of the film. Additional data are given in the report by Charwat *et al.* (1970).

2. Experimental equipment

The rotating disk (38 cm in diameter) is made of optical glass. Liquid is allowed to flow out of a nozzle located over the centre of rotation. The nozzle has a diameter of 0·55 cm and its height is adjusted so that the boundary of the free jet coming out of the nozzle turns smoothly to form the free surface of the film. A second configuration in which the liquid is admitted from below through the shaft was also used. The flow rate is measured by a bank of calibrated flow meters; the rotational speed of the disk is determined by an optical tachometer.

Measurements of local film thickness are made by infra-red absorption. A light source is mounted on a movable arm above the disk, and either steady or modulated light can be used, resulting, respectively, in a direct or alternating electrical signal from the receiving photocell (mounted below the disk). The d.c. method gives some information on the shapes and amplitudes of the waves of the film; the a.c. method improves drift problems in mean-thickness measurements. The output of the photocell is amplified and recorded, using a voltage-to-frequency converter and pulse counter. This signal processing is necessary in order to obtain reproducible mean readings which average the large amplitude irregular waves which often cover the film. The readings so obtained are a logarithmic average of the film thickness. Tests were made with an exponential amplifier incorporated in the apparatus but no significant correction was found within the scatter of the data. The equipment is calibrated directly using a calibration cell which consists of two glass plates (of thickness and quality equal to that of the experimental disk) with a wedge-shaped space of known geometry between them, filled with the test liquid. Film surface conditions were recorded photographically by an overhead camera triggered once each revolution by cams on the shaft. Also, high-speed film sequences were made. A parallel-beam lighting system illuminates the disk.

Prior to each test the disk was washed with soap, ether and acetone and rinsed

with distilled water. The test fluid was stored in a closed head tank and exposed to the normal atmosphere in the laboratory only while on the disk.

Typical ranges of operation of the equipment are as follows. Measurements can be made at radii larger than 2·5 cm, which is the radius of the central nozzle assembly. The maximum flow rate is 13 c.c./s; below 0·3 c.c./s the source nozzle tends not to flow full. Rotational speeds are between 1 and 18 rev/s; the direction of rotation is clockwise looking from above (as on the photographs shown in this paper). The Reynolds number, based on the thickness of the film and the surface velocity, varies from a maximum of about 200 (near the axis) to about 1. In this range we never observed any evidence of microturbulence (such as turbulent 'spots'). The film thickness varies from about 150 μm to approximately 1 μm. The range of radial velocities at the surface of the film is 1–150 cm/s.

3. Mean characteristics of the film

When the flow is laminar and the film sufficiently thin (large values of the radius), the film flow is quasi-parallel and the film's circumferential velocity component v is approximately equal to ωr, where ω is the angular velocity. The radial flow in the film is then described (see Aroesty *et al.* 1967) by the following inertia-free balance† between the local shear and centrifugal forces:

$$\nu d^2u/dz^2 = -\omega^2 r. \tag{3.1}$$

This equation is integrated subject to the no-slip condition at the disk surface and the matching of the surface velocity and shear stress at the interface between the liquid film and the ambient air ($u = u_\delta$ and $\tau = \tau_\delta$ at $z = \delta$, see equation (3.5)). We shall first present results based upon the assumption that the interfacial shear is negligible ($\tau_\delta = 0$); these provide a convenient framework for correlating data. The effect of the air boundary layer over the film will be discussed subsequently.

The radial velocity distribution across the film is found to be parabolic:

$$u = \frac{r\omega^2\delta^2}{\nu}\left[\frac{z}{\delta} - \frac{1}{2}\left(\frac{z}{\delta}\right)^2\right]. \tag{3.2}$$

The maximum radial velocity occurs at the free surface and is

$$u_\delta = \frac{1}{2}\left(\frac{3}{2\pi}\right)^{\frac{2}{3}}\left(\frac{\omega^2 Q^2}{r\nu}\right)^{\frac{1}{3}}, \tag{3.3}$$

where Q is the volumetric flow rate, and the average over the film is

$$\bar{u} = \tfrac{2}{3}u_\delta. \tag{3.4}$$

The tangential velocity in inertial co-ordinates is constant throughout the film; that is, the circumferential velocity in co-ordinates rotating with the disk is zero (to lowest order). The thickness of the film is

$$\delta = \left(\frac{3}{2\pi}\frac{Q\nu}{\omega^2 r^2}\right)^{\frac{1}{3}} \tag{3.5}$$

† Valid for low values of the Rossby number $\bar{u}/\omega r$.

and the pressure in the film is hydrostatic. This far-field solution does not depend on the surface tension. Indeed, from (3.5) it can be seen that the curvature of the surface ($d^2\delta/dr^2$) vanishes like $r^{-\frac{8}{3}}$. This solution contains a characteristic length

$$l = \left(\frac{9}{4\pi^2}\frac{Q^2}{\nu\omega}\right)^{\frac{1}{4}} \tag{3.6}$$

and can be expressed as a function of the dimensionless variables

$$r^* = r/l, \quad \zeta = \frac{z}{\delta} = z\left(\frac{\omega}{\nu}\right)^{\frac{1}{2}} r^{*\frac{2}{3}}. \tag{3.7}$$

Professor J. D. Cole has shown that the above far-field solution is the first term of an asymptotic expansion in $r^* = r/l$ of a solution of the full Navier–Stokes equations. Higher order terms of the series are worked out in detail in another paper (Rauscher *et al.* 1972), where the velocity distribution across the film is given in terms of lengthy polynomials in ζ. These distributions are virtually unmeasurable and, for this reason, only the simpler expressions evaluated at the surface ($\zeta = 1$) are given here.

$$u_\delta/\omega l = \tfrac{1}{2}r^{*-\frac{1}{3}} + (-0{\cdot}111 + 0{\cdot}232 g\nu/Q\omega^2)\, r^{*-3} + O(r^{*-\frac{11}{3}}). \tag{3.8}$$

$$(v_\delta - \omega r)/\omega l = -0{\cdot}417\, r^{*-\frac{5}{3}} + (-0{\cdot}128 + 0{\cdot}199 g\nu/Q\omega^2)\, r^{*-\frac{13}{3}} + O(r^{*-5}) \tag{3.9}$$

$$w_\delta/(\omega\nu)^{\frac{1}{2}} = -\tfrac{1}{3}r^{*-2} + (-0{\cdot}188 + 0{\cdot}466\, g\nu/Q\omega^2)\, r^{*-\frac{14}{3}} + O(r^{*-\frac{16}{3}}), \tag{3.10}$$

$$\delta/(\nu/\omega)^{\frac{1}{2}} = r^{*\frac{2}{3}} + (0{\cdot}197 - 0{\cdot}465 g\nu/Q\omega^2)\, r^{*-\frac{10}{3}} + O(r^{*-4}). \tag{3.11}$$

One can see from (3·8) and (3·9) that the departure of the azimuthal velocity component from solid-body rotation is of $O(r^{*-\frac{4}{3}})$ relative to the leading term of the radial flow. This is proportional to the inverse of the Ekman number E ($E^{-1} \sim \omega\delta^2/\nu$) and arises from the Coriolis acceleration. It is now clear that the second term in each expansion is of $O(E^{-2})$ relative to the leading term, except for the factor involving gravity. This factor can easily be shown to be proportional to the square of an inverse Froude number ($g\delta/\bar{u}^2$) when the leading terms in δ and $\bar{u}$ are used in the definition. The second terms in the expansions arise from the advective and Coriolis terms in the equations of motion and also from the fact that the free-surface stress conditions are applied at a curved surface. The latter effect would also lead at $O(r^{*-\frac{2}{3}})$ to a pressure term which is dependent upon surface tension. One can also show that the vertical velocity is $O(ERo)^{-1}$ relative to the leading term of the radial velocity, where Ro is the Rossby number ($\bar{u}/\omega\delta$), which is a measure of the importance of advection to Coriolis acceleration. The solution carries no information on the outflow from the source other than the magnitude of the flow rate.

A comparison of (3.5) and (3.11) shows that the thickness of the film is virtually unaffected by the second term in the range of the present tests ($r^* \gg 1$). Conversely, the angle of the flow relative to the radius (in co-ordinates rotating with the disk) is a sensitive measure of the degree of approach to the far-field flow. Figures 1 (*a*)–(*c*) show experimental data compared with the leading terms of (3.8) and (3.9). Measurements were obtained as follows. A thin needle was mounted

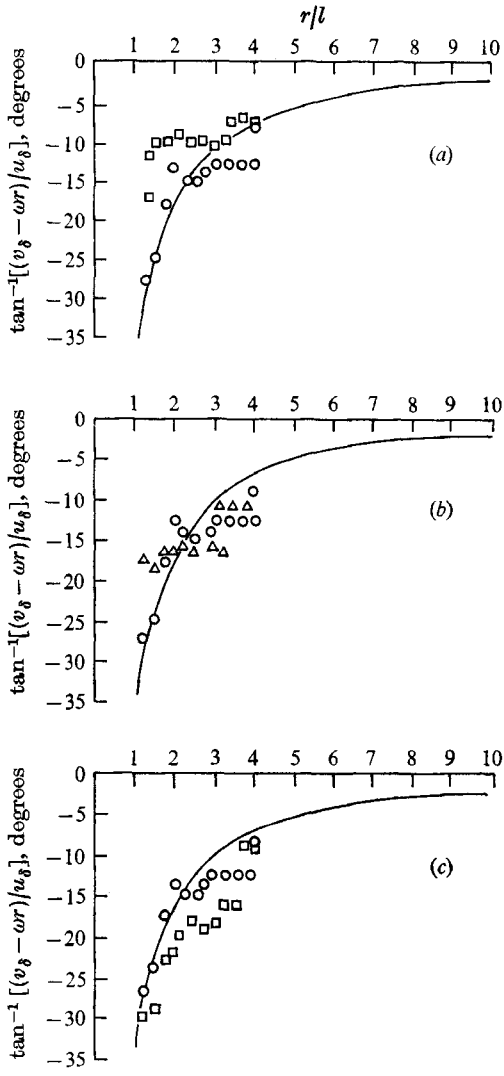

FIGURE 1. Angle of flow at the surface of the film, $\nu^* = 1{\cdot}0$ (ν^* = ratio of kinematic viscosity to that of distilled water). (*a*) $\omega' = 4$ rev/s; ○, $Q = 3{\cdot}33$ c.c./s; □, $Q = 1{\cdot}67$ c.c./s; $\sigma^* = 0{\cdot}85$ (σ^* = ratio of surface tension coefficient to that of distilled water). (*b*) ○, $\omega' = 4$ rev/s; △, $\omega' = 8$ rev/s; $Q = 3{\cdot}33$ c.c./s; $\sigma^* = 0{\cdot}85$. (*c*) $\omega' = 4$ rev/s; $Q = 3{\cdot}33$ c.c./s; ○, $\sigma^* = 0{\cdot}85$; □, $\sigma^* = 1{\cdot}0$.

above the disk on a bar rotating with it and lowered until it just pierced the surface of the film. The disturbance caused a wake, which was photographed. The angle of the line of symmetry of this wake evaluated immediately downstream of the disturbance is the angle of the surface streamline (in rotating co-ordinates). The data is uncertain only to the extent that the needle penetrates the film, across which the flow direction changes, an effect which we believe to be negligible. Additional evidence that the flow relative to the disk is not radial is found in pictures of the shape of dry spots, which are discussed later in this paper.

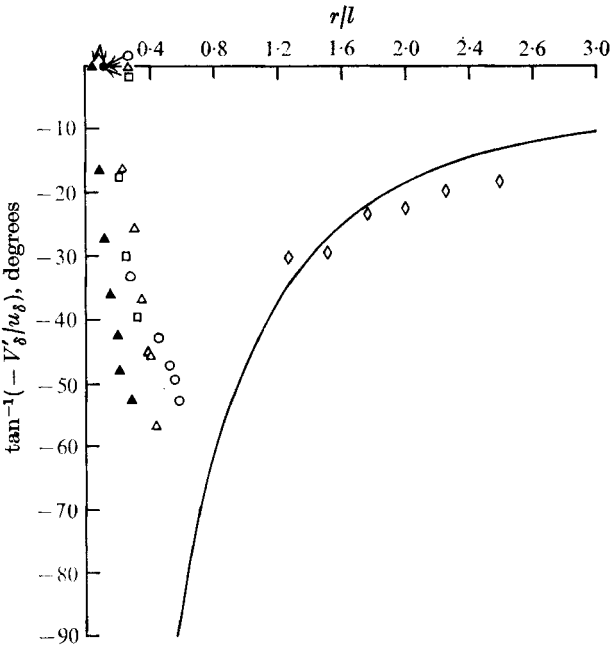

FIGURE 2. Comparison with Dorfman's results. $\nu^* = 1{\cdot}0$, $\sigma^* = 1{\cdot}0$; ——, two-term asymptotic theory; ◇, experimental data.

		$u_0/r\omega$	$\delta^2\omega/\nu$
Numerical results of Dorfman	○	0·5	10
	□	1·5	10
	△	2·5	10
	▲	2·5	50

The region close to the origin must be influenced by the source. An estimate of the extent of this influence can be made by comparing our data with the results of Dorfman's numerical calculations (Dorfman 1967). This is shown in figure 2. In the present experiments the liquid flowed out of a stationary nozzle with out pre-rotation. Dorfman began his integration from an arbitrary, fully pre-rotated profile near the origin. In any case, it appears that the influence of the source decays when $r^* = r/l$ is of order unity.

Figure 3 shows typical measurements of the radial distribution of the mean (time-averaged) film thickness. Both figures 3(*a*) and 3(*b*) show the data correlated in terms of parameters derived from the lowest order asymptotic solution. Figure 3(*b*) gives data for water with enough surface-tension reducing agent to eliminate surface waves (the stability of the surface will be discussed below). Figure 3(*a*) contains measurements made in distilled water and a water–glycerine mixture to change the viscosity. The film surface was mostly covered by waves, hence the larger scatter of the data. Different source positions are included to show the absence of their influence.

It is clear that the grouping of parameters suggested by the asymptotic theory correlates the measurements well with respect to independent variations in the properties of the fluid and the flow. The two-term asymptotic solution gives the

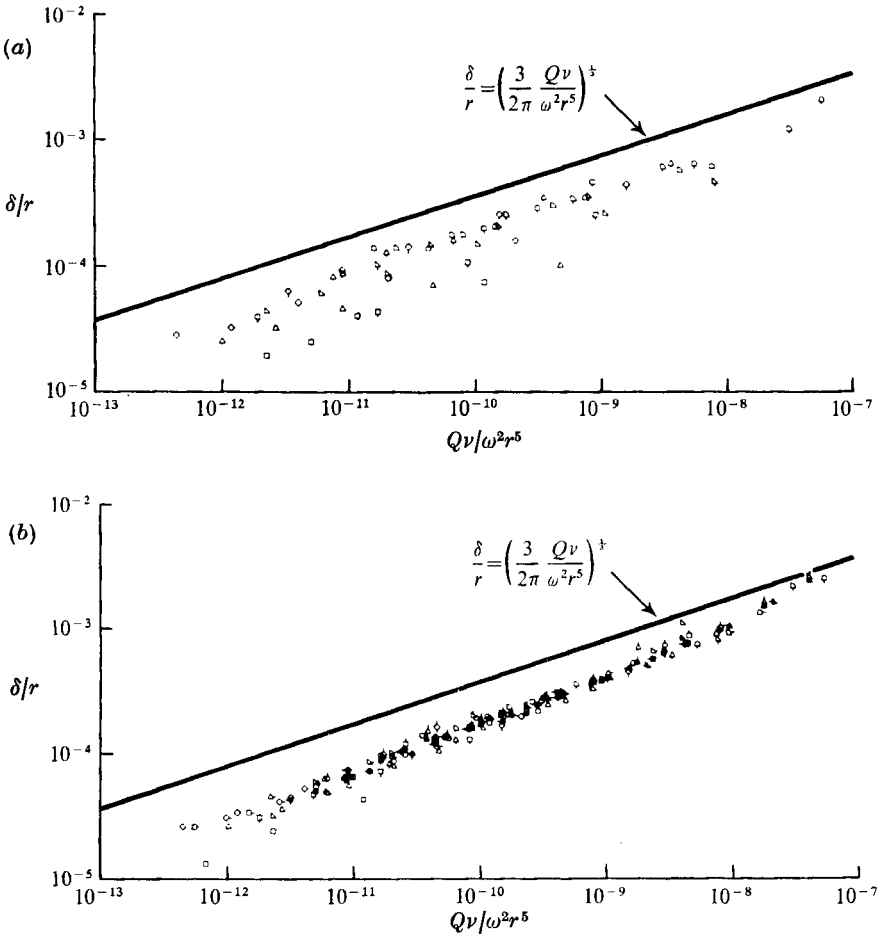

FIGURE 3. Correlation of film-thickness measurements. ○, 15 rev/s; □, 12; ◇, 9; △, 6; ◺, 4; ◺, 2; ⌓, 1·5. Flags giving flow rates in c.c./s: none, 0·20; ◔, 0·41; ◔, 1·28; ◔, 3·71; ◔, 6·93. (*a*) Water and water–glycerine ($\sigma^* = 1$, $1 \leqslant \nu^* \leqslant 2{\cdot}6$). (*b*) Water with wetting agent ($\nu^* = 1$, $1 \leqslant \sigma^* \leqslant 0{\cdot}7$).

direction of the flow remarkably well; this should be a sensitive check on the agreement between theory and data. Nonetheless, measured film thicknesses are systematically lower than those predicted by this analysis. Espig & Hoyle (1965) measured a maximum film thickness, that is, the thickness beneath the crests of the waves which were always present under the conditions of their experiments, and found it to be about 40 % larger than the value given by equation (3.5). If the estimated height of the waves is taken into account, these measurements suggest a mean thickness within 10 % of the theory. The present measurements obey the empirical correlation

$$\delta/r = 1{\cdot}6(Q\nu/\omega^2 r^5)^{0{\cdot}4} \tag{3.12}$$

and cover the range $10^{-12} < Q\nu/\omega^2 r^5 < 10^{-7}$, $1{\cdot}7 < r/l < 20$. In mid-range, they indicate a film with one-half the thickness predicted by (3.5).

The deviation of the measured film thicknesses from those predicted, especially for the larger value of radius at which the asymptotic solution should hold, suggests that the shear stress exerted by the induced air flow might be important. In order to assess this, we can assume that the previous results represent the lowest order solution in an expansion involving the ratio of the viscosity of air to that of the liquid (μ_a/μ_l). With the surface velocities prescribed (equations (3.8) and (3.9)), the air flow can, in principle, be calculated; the shear stress exerted on the liquid would then be known. In order to obtain an estimate it is convenient to assume that the surface velocities relative to the disk are small enough for the classical solution for the flow induced by a rotating disk (Schlichting 1960, p. 83) to be applied. Using that solution, the maximum value of the radial component of the air flow $\approx 0{\cdot}181\omega r$, and the resulting estimate for the shear stress should be good if

$$u_{a\,\max}/u_\delta = 0{\cdot}362(\nu_l/\omega\delta^2) = 0{\cdot}362E \gg 1, \tag{3.13}$$

where E is the Ekman number, which varies as $(r/l)^{\frac{1}{3}}$ on the basis of the previous solution. For $E \approx 30$ the estimate should be good. Although this corresponds to very thin films, the estimate should, at any rate, be conservative because the interfacial stress will be less for smaller values of E. Assuming that (3.13) is satisfied, we can say that

$$\tau_\delta = \mu_a(0{\cdot}510\, r\omega)\,(\omega/\nu_a)^{\frac{1}{2}} \tag{3.14}$$

and use this as a boundary condition in solving (3.1). We then find that

$$u_\delta = \frac{r\omega^2\delta^2}{2\nu_l} + \delta\left(\frac{\mu_a}{\mu_l}\right)(0{\cdot}510\, r\omega)\left(\frac{\omega}{\nu_a}\right)^{\frac{1}{2}} \tag{3.15}$$

and, from the volumetric flux condition,

$$\delta = \left(\frac{\nu_l}{\omega}\right)^{\frac{1}{2}}\left(\frac{l}{r}\right)^{\frac{3}{8}}\left[1 - 0{\cdot}255\left(\frac{\mu_a}{\mu_l}\right)\left(\frac{\nu_l}{\nu_a}\right)^{\frac{1}{2}}\left(\frac{r}{l}\right)^{\frac{3}{8}} + O\left(\frac{\mu_a}{\mu_l}\right)^2\right]. \tag{3.16}$$

This indicates that the film thickness will be decreased owing to the induced air flow. However, even for $(r/l) \sim 55$ the correction is only about 1·5 %, so that, although consideration of the induced air flow gives the correct qualitative behaviour, the discrepancy between experiment and the free-surface solution cannot be explained on this basis. We might also note that for low values of E (3.13) suggests that the air flow might tend to decrease the film velocity, which would then tend to thicken the film relative to the free-surface solution. Using the result (3.16) in (3.15), we find that

$$\frac{u_\delta}{\omega l} = \tfrac{1}{2} r^{*-\frac{1}{3}}\left[1 + 0{\cdot}510\left(\frac{\mu_a}{\mu_l}\right)\left(\frac{\nu_l}{\nu_a}\right)^{\frac{1}{2}} r^{*\frac{3}{8}} + O\left(\frac{\mu_a}{\mu_l}\right)^2\right], \tag{3.17}$$

so that the correction to the radial component of the surface velocity is again typically small. However, if we again use the classical solution in order to compute the effect of the air flow upon the azimuthal velocity, then we find (cf. equation (3.9)) that

$$\frac{v_\delta - \omega r}{\omega l} = -0{\cdot}417 r^{*-\frac{5}{3}}\left[1 + \left(\frac{\mu_a}{\mu_l}\right)\left(\frac{\nu_l}{\nu_a}\right)^{\frac{1}{2}}\left\{\frac{0{\cdot}616}{0{\cdot}417} r^{*2} - 1{\cdot}020 r^{*\frac{3}{8}}\right\} + O\left(\frac{\mu_a}{\mu_l}\right)^2\right], \tag{3.18}$$

where the first term in parentheses represents the effect of the induced stress and the second represents the change in δ. It is clear that the effect of the air upon the azimuthal flow is more important than the effect upon the radial flow for large r^*. For $r^* \approx 4$ the correction to the azimuthal flow is about 10%, whereas the correction to the radial flow is insignificant. This might explain the tendency for the data in figure 1 to fall somewhat below the predicted curve.

4. Characteristics of surface waves

Figure 4 (*a*) (plate 1) shows completely steady flow over the entire disk. Figure 4 (*b*) (plate 1) shows the existence of a train of concentric waves near the centre of the disk. These waves move outward and decay, and the outer part of the film is smooth. Figure 4 (*c*) (plate 1) shows a pattern of spiral waves. These waves seem to be fixed to the rotating disk (they are stationary in the rotating co-ordinate system) and unwind in the direction of rotation. They tend to decay at large radii but, in most cases, they first break up into a very rough and non-uniform pattern of disconnected wedge-like wavelets (figure 4 (*d*) (plate 1) c.f. Tailby & Portalski 1962, figure 9).

The occurrence of waves of either type depends on the magnitude of all four experimental variables: the flow rate Q, the rotational speed ω, the surface tension of the fluid σ and the fluid viscosity ν. Figure 5 is a plot of the stability boundaries of both families of waves. To the left of the limit curve labelled 'concentric waves' such waves are seen† always near the centre of the disk. To the right of a curve labelled 'spiral waves', depending on the value of σ, spiral waves are seen, always starting at some radius away from the centre. Between the 'concentric' and 'spiral'-wave limit curves the film is completely smooth. In regions above the point of intersection of these curves (for given σ and ν) both types of waves are present, so that their nature is no longer clear.

Figure 6 (plate 2) shows oscilloscope traces‡ of the output of the film-thickness measuring photocell in the regime of concentric waves, spiral waves and also, for comparison, across a 'dry spot'. There is clearly a substantial difference in the character of the two families of waves: the concentric waves form a sinusoidal train of small amplitude disturbances, while the spiral waves are large and exhibit sharp peaks and shallow troughs. This data is qualitative because the logarithmic response of the instrument depresses the wave peaks (large local film thickness) relative to the troughs. Also, the instrument cuts the waves along a constant radius. The period of the spiral wave traces is a projection of their wavelength on a plane at the local angle of the spiral (stationary waves). The period of the concentric wave traces is related to their wave speed.

In order to provide a framework for the discussion of the data an attempt was made to extend the linear stability theory for thin planar films to the present case (Rauscher 1969). It is shown that the stability equation (Orr–Sommerfeld

† Since the nozzle assembly obscured the centre, this line represents conditions where no concentric waves are visible beyond $r = 2$ cm.

‡ For these tests the light source was operated on continuous current and the photocell output was a.c. coupled to the oscilloscope. The electronic signal amplification was the same in all cases.

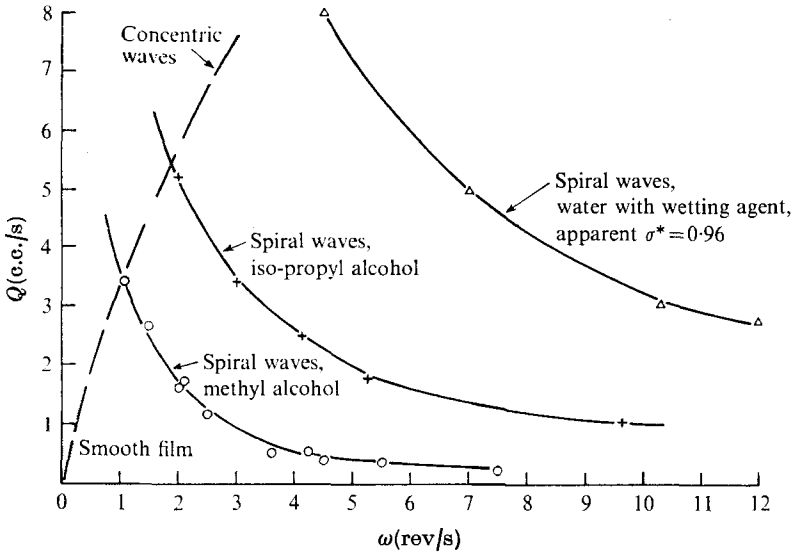

FIGURE 5. Boundaries of concentric and spiral waves.

Parameter	Definition	Significance	Expression in terms of laboratory parameters	Experimental range
Re: Reynolds number	$\frac{\bar{u}\delta}{\nu}$	$\frac{\text{Inertia}}{\text{Viscosity}}$	$\frac{1}{2\pi}\left(\frac{Q}{r\nu}\right)$	1–150
We: Weber number	$\frac{\sigma/\rho}{\delta\bar{u}^2}$	$\frac{\text{Surface tension}}{\text{Inertia}}$	$9\left(\frac{2\pi}{3}\right)^{\frac{5}{3}}\left(\frac{\sigma^3\nu r^4}{\rho^3 Q^5\omega^2}\right)^{\frac{1}{3}}$	$0{\cdot}4$–10^3
E: Ekman number	$\frac{\nu}{\omega\delta^2}$	$\frac{\text{Viscosity}}{\text{Coriolis}}$	$\left(\frac{2\pi}{3}\right)^{\frac{2}{3}}\left(\frac{\nu\omega r^4}{Q^2}\right)^{\frac{1}{3}}$	$0{\cdot}4$–100
F^{-2}: Inverse Froude number	$\frac{g\delta}{\bar{u}^2}$	$\frac{\text{Gravity}}{\text{Inertia}}$	$6\pi\left(\frac{g\nu}{\omega^2 Q}\right)$	$0{\cdot}05$–$3{\cdot}0$
Ro: Rossby number ($E\,Re$)	$\frac{\bar{u}}{\omega\delta}$	$\frac{\text{Inertia}}{\text{Coriolis}}$	$\frac{1}{3}\left(\frac{3}{2\pi}\right)^{\frac{1}{3}}\left(\frac{Q\omega r}{\nu^2}\right)^{\frac{1}{3}}$	10–200

TABLE 1. Scaling parameters

equation) and the associated boundary conditions for a two-dimensional disturbance to the planar film† and for an axisymmetric disturbance to the spinning film are identical to order $r^{*-\frac{1}{3}}$. These results are obtained by expanding about a local position so that, at any point on the rotating disk, the stability of the film corresponds to that on a plane having an inclination $\epsilon = \cot^{-1}(g/\omega^2 r)$ to the horizontal (Binnie 1957). To this order the effect of Coriolis forces on both the disturbance and the mean flow are neglected. These forces, which act in the plane of the disk, must be associated with the appearance of oblique (spiral) waves. In

† Rauscher compares the rotating disk to the planar film on vertical planes and finds these problems to be equivalent when a term involving gravity is small. This term transforms exactly into the term representing the influence of inclination of the plane to the horizontal.

order to discuss this phenomenon the stability of a simplified pseudo two-dimensional model of the rotating film is described later in this paper. This analysis provides a guide for the following discussion of the measurements, but it is essential to bear in mind certain fundamental shortcomings of the theoretical model. The analysis is formally valid only at large radii (large values of r^*, i.e. large Ekman numbers) and small amplitude waves. Furthermore, expansions about a *local* position neglect the radial variation of the flow properties and their effect on the *history* of the disturbance. The observed waves have large amplitude and therefore have a history. Table 1 summarizes the dimensionless scaling parameters which govern the flow and gives them in terms of variables measured in the laboratory. It can be seen that, unlike plane film flow, for which these parameters remain constant in space, the Reynolds number decreases with radius while the Weber and Ekman numbers increase with it. The Froude number is not a function of radius. For instance, the assumption made usually, that the characteristics of the observed waves are those of the locally most highly amplified small disturbances, is less justifiable than in the case of plane films, and nonlinear effects, such as the 'locking in' of waves once they become large, may be important.

4.1. *Characteristics of the concentric waves*

The concentric waves originate at the nozzle and decay with radius. We believe that the waves are generated by the nozzle outflow, possibly owing to the highly curved free surface of the jet as it turns out to spread out on the disk. They should not be identified with the two-dimensional waves observed on an inclined plane, which find their true counterpart as a limiting case of the spiral waves for very large Ekman numbers. The axial symmetry of the waves is imposed in this case by the axial symmetry of the source and only in part by the stability properties of the film.

The wavenumber of the concentric waves, based on conditions a short distance ahead of the radius at which they cease to be visible, is plotted on figure 7. It is not possible to ascertain accurately whether the wavelength of the wave train is constant or whether it varies as δ varies over the range of radii where they are visible. The wave speed, which can be estimated from oscilloscope records such as those shown in figure 6, is about twice the surface speed (ranging between 1·7 and $2{\cdot}8u_s$). The wave speed and the wavenumber of the concentric waves is quite close to those of the most highly amplified long waves according to linear theory for planar films on a vertical wall (Benjamin 1957); figure 7 also shows these wavenumbers for comparison.

Small disturbance theory for axisymmetric waves predicts that the film should be unstable in this range of wavenumbers and Weber and Froude numbers. The fact that the observed concentric waves decay might seem to be surprising. The theoretical model discussed below shows that the Coriolis force has no effect upon axisymmetric disturbances. However, this conclusion is only valid for the large E for which the theory is valid, i.e. large radii with fixed flow conditions. For large E the lowest order azimuthal disturbance velocity only exists because of the mean azimuthal shear, which becomes of $O(E^{-1})$ for an axisymmetric disturbance. Hence, the Coriolis effect upon the axisymmetric disturbance owing

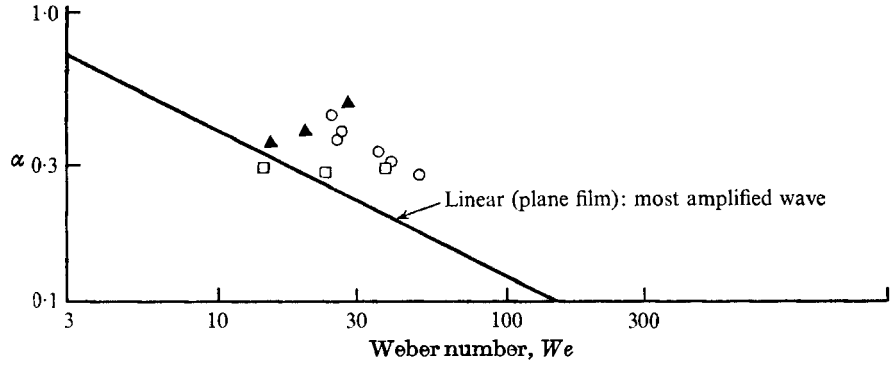

FIGURE 7. The wavenumber of concentric waves. □, $\nu^* = 1$, $\sigma^* = 0{\cdot}83$; ○, $\nu^* = 1{\cdot}0$, $\sigma^* = 0{\cdot}96$; ▲, $\nu^* = 2.6$, $\sigma^* = 0{\cdot}85$.

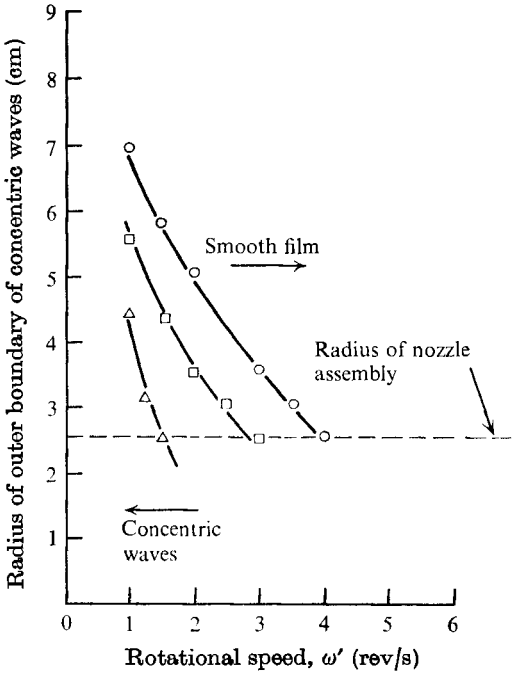

FIGURE 8. Example of the radius of decay of concentric waves in distilled water. ○, $Q = 12{\cdot}0$ c.c./s; □, $Q = 8{\cdot}33$ c.c./s; △, $Q = 5{\cdot}00$ c.c./s.

to the perturbed azimuthal flow becomes less important. In the region of decay of the concentric waves the Ekman number varies between 0·5 and 2·5. For E of order unity the disturbance equations are coupled and the azimuthal disturbance velocity is of the same order as the radial disturbance velocity, and so the Coriolis force can have a stronger influence. Because the concentric waves exist under conditions for which they would seem likely to extract energy from the mean radial flow (again, on the basis of the large E analysis), we suggest that the Coriolis force might have a stabilizing influence upon these (imposed) concentric waves. With this in mind, we note that the asymptotic analysis does

predict that the growth rate of an oblique wave is less when the direct effect of the Coriolis force upon the disturbance is included than when only its indirect effect in creating a non-unidirectional mean flow is considered.

Figure 8 shows an example of the variations in the radius at which the concentric wave train disappears. The initial magnitude of the waves (which we suppose to be dependent on the configuration of the outflow from the nozzle) seems to increase with the flow rate (for fixed geometry of the nozzle) and with decreasing surface tension; this seems reasonable. The rate of decay of the waves increases with rotational speed and decreases with flow rate (which indicates that it increases with decreasing film thickness).

4.2. *Characteristics of the spiral waves*

Figure 9 shows measurements of the spiral angle plotted against the Ekman number and compared with the angle of the most unstable wave as predicted by the analysis given in the following section. The correlation is quite good. Changes in the surface tension of the liquid (the Weber number) and surface-tension-reducing activities do not seem to affect this angle. This too is verified by the analysis. The spiral angles are negative, corresponding to a spiral which unwinds in the direction of rotation. Observations suggest that the spiral is stationary in a frame rotating with the disk but we were unable to determine this with certainty. High-speed photography at 3000 frames per second was used to follow the radial location of a wave crest in intervals of a few degrees. The stability analysis indicates, on the other hand, that the wave speed of these waves (negative β) is finite and increases somewhat with their obliqueness.

The wavenumber of the spiral waves appears to be nearly constant (figure 10). The Reynolds number is used as the ordinate only as a means of displaying the data. The wavelength on which this wavenumber is based refers to the radial spacing between successive waves in a wave packet and is not to be confused with the radial distance separating successive passes of the same spiral through a fixed circumferential station. When the flow conditions are near the stability limit, we can often see a single spiral or packets of two or three waves spiralling around the disk with smooth flow between the passes. In these cases the waves are well defined and often decay without breaking up into disconnected three-dimensional wavelets. Such a breakup occurs when the film is more unstable and 'full' of waves. It may be due, in part, to a geometric interference between the waves, but, noting that this breakup of waves is also observed in plane flow, it is more likely to be due to the (nonlinear) instability of the wave itself. The 'random' wavelets also decay with radius; we could not determine their motion relative to the disk.

The radius at which the spiral waves originate and the approximate radius at which all waves cease to be visible is shown on figure 11 for water and a water–glycerine mixture. The minimum value of the product $Q\omega$ on figure 11 (empirically, the dominant simple combination of parameters) below which no spiral waves are seen at any radius corresponds to the curve displayed on figure 5. The origin of the waves can be determined fairly accurately; the radius of their decay is more uncertain because in the majority of cases the waves 'break up'

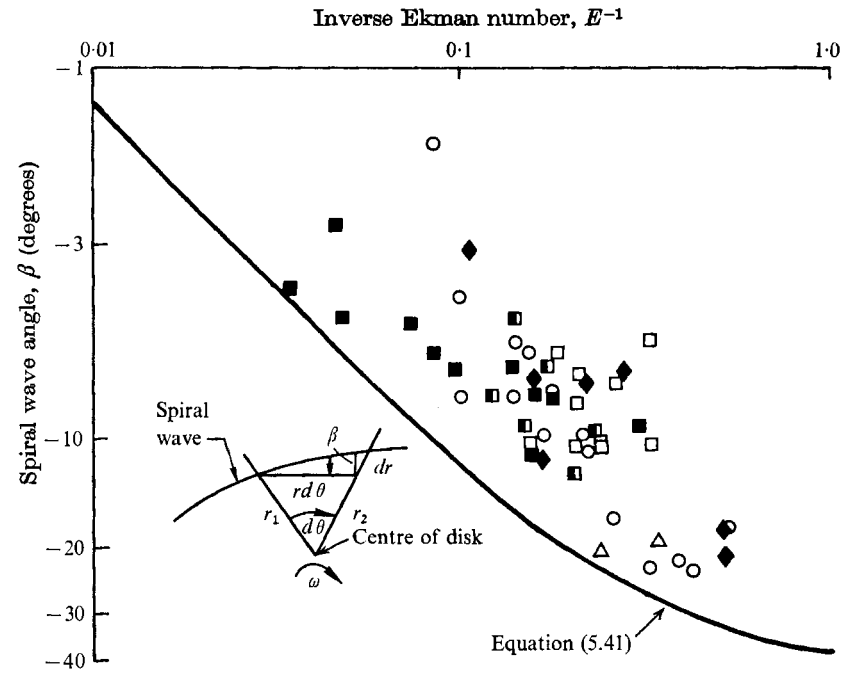

FIGURE 9. The angle of the spiral waves, $-\beta = \tan^{-1}[(1/r)(dr/d\theta)]$.

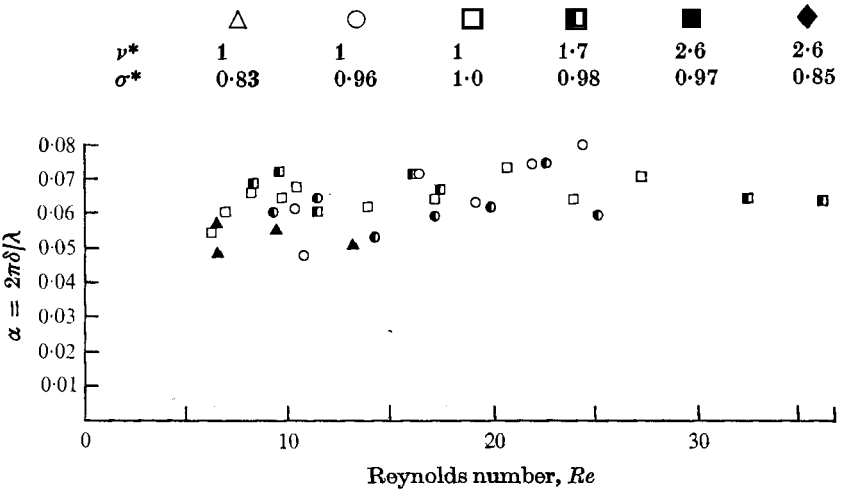

FIGURE 10. Wavenumber of spiral waves. ▲, $\nu^* = 2{\cdot}6$, $\sigma^* = 0{\cdot}85$. For $\sigma^* = 1$, $\nu^* = 1$: ○, $\omega' = 4$ rev/s, $r = 7{\cdot}52$ cm; ◐, $\omega' = 6$ rev/s, $r = 7{\cdot}52$ cm; □, $\omega' = 9$ rev/s, $r = 4{\cdot}73$ cm; ◧, $\omega' = 12$ rev/s, $r = 4{\cdot}73$ cm.

first and the disappearance of the random wavelets is difficult to specify. The general aspect of the spiral-wave boundaries and their variation with Q and ω is the same for all liquids tested (water; water–glycerine mixture; propyl, ethyl and methyl alcohols).

Because the stability analysis of the following section is restricted to large values of E (i.e. large radii), it is not suited for predicting the radius at which the

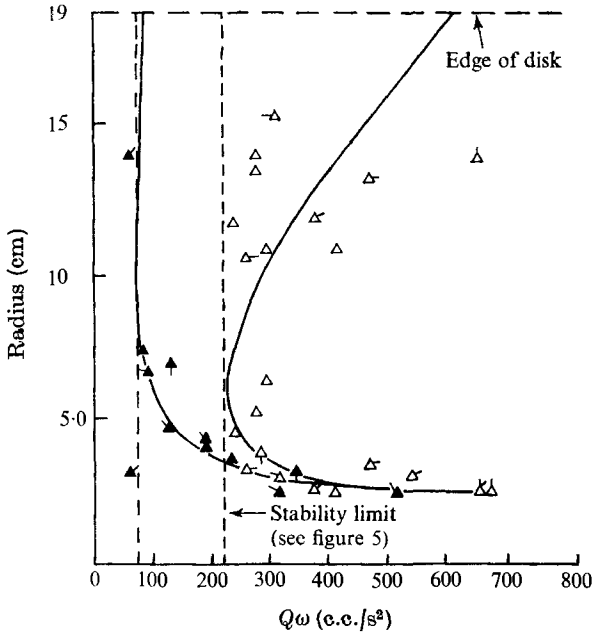

FIGURE 11. Domain of spiral waves. △, $\nu^* = 1{\cdot}0$, $\sigma^* = 0{\cdot}96$; ▲, $\nu^* = 2{\cdot}6$, $\sigma^* = 0{\cdot}97$. Flags: none, $\omega' = 4$ rev/s; ♀, $\omega' = 6$ rev/s; ♂, $\omega' = 8$ rev/s; ♉, $\omega' = 9$ rev/s; ♌, $\omega' = 10$ rev/s; -○, $\omega' = 12$ rev/s; ♁, $\omega' = 14$ rev/s; ♂, $\omega' = 16$ rev/s.

spiral waves appear. On the other hand, it is felt that the analysis should give a reasonable description of the amplification rate of the waves while they travel through a substantial part of the unstable region. Hence it can be employed to parametrize the total amplification of a wave, which is a measure of whether or not a wave is observed.

The amplification of a wave is

$$A \sim \exp\left\{\int^1 \left(-\frac{\alpha_i}{\delta}\right) r_0 \, d(r/r_0)\right\} \sim \exp\left\{\frac{\bar{u}_0 r_0}{\nu}\int^1 \left(-\frac{\alpha_i}{Re}\right)\left(\frac{\bar{u}}{\bar{u}_0}\right) d(r/r_0)\right\}, \qquad (4.1)$$

where $-\alpha_i$ is the local non-dimensional spatial amplification rate, r_0 is a length scale characteristic of the unstable region and $\bar{u}_0 = \bar{u}(r_0)$. The lower limit of the integral is not specified. Now it is known that for low amplification $-\alpha_i \cong (\alpha c_i/c_g)$, where $(\alpha c)_i$ is the temporal growth rate and c_g is the group velocity, which is approximately equal to the phase velocity in the present case. Using the result for the growth rate (equation (5.40)), we have

$$-\frac{\alpha_i}{Re} = \alpha^2\left[\frac{\frac{6}{5}\cos^2\beta - \frac{1}{3}(\alpha^2 We + 1/F^2) - (2{\cdot}571/E)\sin 2\beta}{3\cos\beta - (4/E)\sin\beta}\right]. \qquad (4.2)$$

For a wave with fixed α, corresponding to those observed, $-\alpha_i$ will approach zero as r increases, because both We and E increase. Now $\tan\beta$ behaves like E^{-1} for large E (cf. (5.41) and figure 9), so the terms involving $\sin\beta/E$ are of $O(E^{-2})$. Because the flow will be stabilized when We is sufficiently large, it is natural to choose r_0 on the basis that $\alpha^2 We \sim O(1)$ or, for fixed α,

$$r_0 = [\rho^3 Q^5 \omega^2/\sigma^3 \nu]^{\frac{1}{4}}. \qquad (4.3)$$

Once this is specified, we can express E^{-2} in terms of r_0:

$$\frac{1}{E^2} \sim \left[\frac{Q^2}{\nu\omega r_0^4}\left(\frac{r_0}{r}\right)^4\right]^{\frac{2}{3}} \sim \Lambda^2\left(\frac{r_0}{r}\right)^{\frac{8}{3}}, \tag{4.4}$$

where

$$\Lambda = \left(\frac{\sigma}{\rho}\right)\left(\frac{1}{Q\omega}\right), \tag{4.5}$$

and state that

$$-\frac{\alpha_i}{Re} = \text{fn}\left\{\left(\frac{r}{r_0}\right), \frac{1}{F^2}, \Lambda\right\}. \tag{4.6}$$

For a film with fixed surface properties, the importance of the value of ωQ is thus evident from the definition of Λ. The remaining parameter defining the total amplification is

$$\frac{\bar{u}_0 r_0}{\nu} \sim \left(\frac{\rho}{\sigma}\right)^{\frac{1}{2}} \frac{Q^{\frac{3}{2}}\omega}{\nu^{\frac{3}{2}}} = \left[\frac{Q^2\omega}{\Lambda\nu^3}\right]^{\frac{1}{2}}, \tag{4.7}$$

so that the final parameter could be $Q^2\omega/\nu^3$. However, the parameters can be combined to yield the set

$$A = A\left\{\frac{1}{F^2}, \frac{\sigma\omega}{\rho\nu g}, \frac{\sigma^{\frac{3}{4}}}{\rho^{\frac{3}{4}}\nu g^{\frac{1}{4}}}\right\}, \tag{4.8}$$

which has the advantage that the final parameter in parentheses is only a function of the properties of the film.

The conditions under which spiral waves are no longer visible are displayed in terms of these parameters in figure 12. For given film properties, the data fall approximately on a straight line having a slope near unity in the plane of

$$F^{-2} \sim \omega^{-2}Q^{-1} \quad \text{and} \quad \omega,$$

which suggests the rough correlation of the stability limit with the product $Q\omega$, as in figure 11.

Figure 12 includes data for pure water which exhibit considerable scatter. This is because at these values of the physical constants the critical ω and Q are very low, at the lower limit of accurate operation of the equipment, and the very thin film tends to form dry spots. We have indicated the line corresponding to water ($\sigma^{\frac{3}{4}}/\rho^{\frac{3}{4}}\nu g^{\frac{1}{4}} = 450$) by a broken line.

Tests were also performed with the addition of a surface-wetting agent (Kodak Photo-Flo) to water and to a water–glycerine mixture (with viscosity 2·6 times that of water). The object was to prevent film breakup for very thin films. By decreasing the surface tension, one would expect that the film would become more unstable. Instead, a pronounced stabilization of the film occurred. In fact, no waves were observed when the following empirical correlation was satisfied:

$$1/Q\omega = r(a - b\rho/\sigma_a), \quad a = 2{\cdot}90\,\text{s}^3\,\text{cm}^{-5}, \quad b = 1{\cdot}65\,\text{dyn}\,\text{s}^3\,\text{cm}^{-6}, \tag{4.9}$$

where σ_a is the 'apparent' surface tension of the mixture as measured by the capillary-rise method. This equation shows that when the apparent surface tension is reduced below about 57 dyn cm^{-1} the film becomes absolutely stable; no waves of any kind could be observed throughout the entire range of flow rates and rotational speeds of which the equipment was capable. It is felt that the

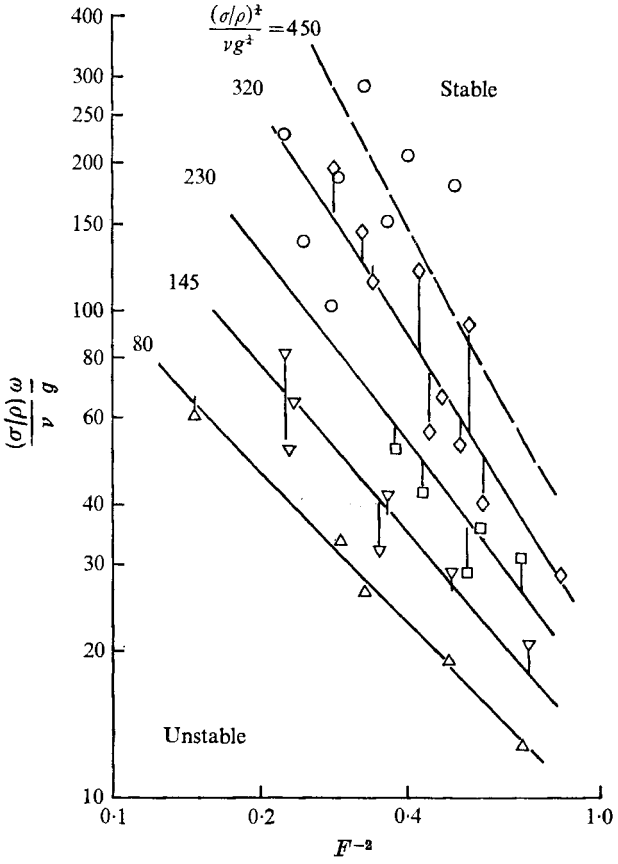

FIGURE 12. Correlation of absolute stability limits for spiral waves in water and methyl, ethyl and iso-propyl alcohol (and their mixtures).

surface-wetting additive gave rise to phenomena associated with surface-active agents, e.g. surface elasticity and surface viscosity. For planar films, both Benjamin (1964) and Whitaker (1964) have shown that surface elasticity can be strongly stabilizing. This is true especially for long waves; Benjamin demonstrated that the stabilizing effect of surface elasticity is independent of wave-number (unlike the effect of surface tension).

Figure 13 shows measurements of the amplitude of spiral waves. These measurements are rather inaccurate but they do show unequivocally that the waves grow to a maximum and then decay. The maximum amplitude of the waves is large, 30–50 % of the local film thickness. The maximum is reached relatively near the beginning of the wave regime but the accuracy of the data is not sufficient to locate it exactly. Figure 13 (*b*) shows the amplitude of the waves at $r = 2{\cdot}5$ in., which is approximately the location of the maximum for the range of flow rates and rotational speeds tested with distilled water. Amplitude data for reduced surface tension were not taken, but the waves are then visibly smaller.

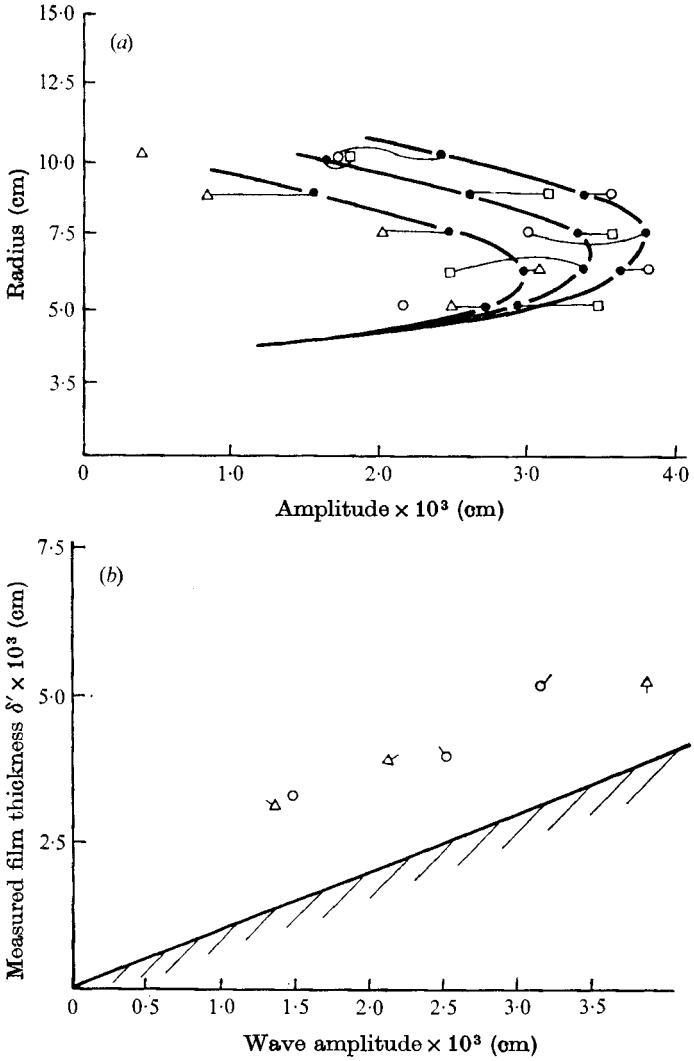

FIGURE 13. Spiral-wave amplitude (distilled water: $\sigma^* = \nu^* = 1$). (*a*) Wave amplitude *vs.* radius at selected flow conditions. ○, Q = 10 c.c./s; □, Q = 6·67 c.c./s; △, Q = 5·0 c.c./s, ω' = 10 rev/s. (*b*) Wave amplitude *vs.* film thickness at constant radius. Distance ◿—○ shows scatter. ○, Q = 10 c.c./s; △, Q = 5 c.c./s; radius = 6·35 cm. Flags: ○, ω' = 4 rev/s; ♂, ω' = 6 rev/s; ♁, ω' = 8 rev/s; none, ω' = 10 rev/s.

5. Analytical model of the stability of a rotating film

The purpose of this study is to investigate, as simply as possible, how rotation might lead to the formation of spiral waves. It is assumed that the Ekman number E is large enough for the asymptotic solution given earlier to be meaningful and for terms of $O(E^{-2})$ to be neglected. This allows us to construct a parallel-flow model which yields the inclined plane stability results as $E \to \infty$. We seek to evaluate the effects of terms of $O(E^{-1})$, which reflect the importance of the Coriolis force. Because we essentially expand about the result for the inclined plane, for

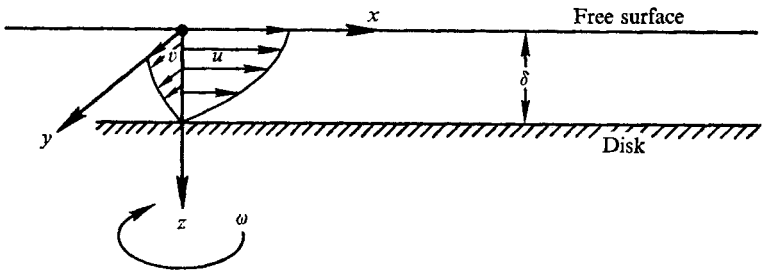

FIGURE 14. Sketch of the co-ordinate system.

which the wave velocity of the most unstable wave is always greater than the maximum flow velocity, we cannot hope to predict the observed spiral waves, which appear to be stationary relative to the disk. Nonetheless, the model does indicate that spiral waves can be expected and serves as a useful vehicle for the discussion of the stability problem.

As shown in figure 14, we consider the motion of a layer of viscous fluid of (constant) depth δ which has a free surface and is bounded below by a wall, and which is acted upon by a constant body force ρB in the x direction. The whole system is rotating with angular velocity ω about the vertical axis, and we consider the motion relative to the rotating frame of reference (positive z is measured downwards from the free surface, so positive ω corresponds to a rotation in the clockwise direction, as viewed from above). The equations which govern the assumed parallel mean flow are

$$-2\omega v = \nu d^2u/dz^2 + B \tag{5.1a}$$

and

$$2\omega u = \nu d^2v/dz^2. \tag{5.1b}$$

Defining an Ekman number as $E = (\nu/\omega\delta^2)$ and further defining

$$z = \delta\zeta, \quad u = u_c U(\zeta), \quad v = u_c E^{-1} V(\zeta), \tag{5.2}$$

where u_c is a characteristic velocity, the equations become

$$-2E^{-2}V = \frac{d^2U}{d\zeta^2} + \frac{B\delta^2}{u_c\nu} \tag{5.3a}$$

and

$$2U = d^2V/d\zeta^2, \tag{5.3b}$$

which are to be solved subject to the conditions of zero slip at the wall and zero shear stress at the free surface. The model can be viewed as being appropriate to a situation in which the body force is large in comparison to the centrifugal force. However, in order to relate our results to the rotating-disk results, we have to identify B with the centrifugal force, so $B \sim O(\omega^2 x)$. By including the body force only in the x momentum equation, we are essentially identifying u with the radial flow and v with the azimuthal flow relative to the disk, at least on a local basis. The parallel-flow model is meaningful only for $E \gg 1$. In this limit, a flow is produced which is predominantly in the direction of the body force. In contrast to Ekman layer flows and the flow induced by a rotating disk in an unbounded fluid, such a quasi-unidirectional model would appear to be appropriate to at

least some of the data obtained with the rotating disk (cf. figure 1), although only in regions far from the origin of the flow. If we ignore terms of $O(E^{-2})$, then the flow components with the present model are identical to the corresponding components in the asymptotic solution for the disk flow. We shall ignore such terms (which reflect the three-dimensional nature of the flow in the disk solution) and take our description of the mean flow as

$$U = (B\delta^2/2\overline{u}_c\nu)(1-\zeta^2) \tag{5.4a}$$

and

$$V = (B\delta^2/\overline{u}_c\nu)(-\tfrac{5}{12}+\tfrac{1}{2}\zeta^2-\tfrac{1}{12}\zeta^4). \tag{5.4b}$$

We now identify u_c with an average velocity in the x direction by stipulating

$$\int_0^1 U\,d\delta = 1, \tag{5.5}$$

so that $u_c = \overline{u} = \delta^2 B/3\nu$.

The stability problem can be easily formulated in our Cartesian system. We make all lengths non-dimensional on the basis of δ and time on the basis of $\overline{u}$ and δ. We let

$$u = \overline{u}(U+\epsilon\hat{u}), \quad v = \overline{u}(E^{-1}V+\epsilon\hat{v}), \quad w = \epsilon\overline{u}\hat{w}, \tag{5.6}$$

where $(\hat{})$ denotes a perturbation quantity dependent on x, y, ζ, and t, and $\epsilon \ll 1$. We write the non-dimensional pressure as

$$p/\rho\overline{u}^2 = (1/F^2)P(\zeta)+\epsilon\hat{p}, \tag{5.7}$$

where $P(\zeta)$ is the hydrostatic distribution ($dP/d\zeta = 1$) and F^{-2} is the square of the inverse of the Froude number. If we introduce a Reynolds number, the continuity and momentum equations for the $O(\epsilon)$ term become

$$\frac{\partial\hat{u}}{\partial x}+\frac{\partial\hat{v}}{\partial y}+\frac{\partial\hat{w}}{\partial\zeta} = 0, \tag{5.8a}$$

$$\frac{\partial\hat{u}}{\partial t}+U\frac{\partial\hat{u}}{\partial x}+E^{-1}V\frac{\partial\hat{u}}{\partial y}+\frac{dU}{d\zeta}\hat{w}-\frac{2}{E\,Re}\hat{v} = -\frac{\partial\hat{p}}{\partial x}+\frac{1}{Re}\nabla^2\hat{u}, \tag{5.8b}$$

$$\frac{\partial\hat{v}}{\partial t}+U\frac{\partial\hat{v}}{\partial x}+E^{-1}V\frac{\partial\hat{v}}{\partial y}+E^{-1}\frac{dV}{d\zeta}\hat{w}+\frac{2}{E\,Re}\hat{u} = -\frac{\partial\hat{p}}{\partial y}+\frac{1}{Re}\nabla^2\hat{v}, \tag{5.8c}$$

$$\frac{\partial\hat{w}}{\partial t}+U\frac{\partial\hat{w}}{\partial x}+E^{-1}V\frac{\partial\hat{w}}{\partial y} = -\frac{\partial\hat{p}}{\partial\zeta}+\frac{1}{Re}\nabla^2\hat{w}. \tag{5.8d}$$

We now model the spiral wave by looking for a solution periodic in some direction x^*, say, which is inclined at an angle β, positive in the clockwise direction from above, to the x axis. Hence, we let

$$x^* = x\cos\beta+y\sin\beta \tag{5.9a}$$

and

$$y^* = -x\sin\beta+y\cos\beta, \tag{5.9b}$$

so that y^* is normal to x^*. If we transform $(\hat{u},\hat{v})$ to $(\hat{u}^*,\hat{v}^*)$ similarly and stipulate that $\partial/\partial y^* \equiv 0$, the continuity equation becomes simply

$$\frac{\partial\hat{u}^*}{\partial x^*}+\frac{\partial\hat{w}}{\partial\zeta} = 0, \tag{5.10a}$$

whereas the momentum equations can be suitably combined to give

$$\frac{\partial \hat{u}^*}{\partial t} + U^* \frac{\partial \hat{u}^*}{\partial x^*} + \frac{dU^*}{d\zeta}\hat{w} - \frac{2}{E\,Re}\hat{v}^* = -\frac{\partial \hat{p}}{\partial x^*} + \frac{1}{Re}\left(\frac{\partial^2}{\partial \zeta^2} + \frac{\partial^2}{\partial x^{*2}}\right)\hat{u}^*, \tag{5.10b}$$

$$\frac{\partial \hat{v}^*}{\partial t} + U^* \frac{\partial \hat{v}^*}{\partial x^*} + \frac{dV^*}{d\zeta}\hat{w} + \frac{2}{E\,Re}\hat{u}^* = \frac{1}{Re}\left(\frac{\partial^2}{\partial \zeta^2} + \frac{\partial^2}{\partial x^{*2}}\right)\hat{v}^*, \tag{5.10c}$$

and

$$\frac{\partial \hat{w}}{\partial t} + U^* \frac{\partial \hat{w}^*}{\partial x^*} = -\frac{\partial \hat{p}}{\partial \zeta} + \frac{1}{Re}\left(\frac{\partial^2}{\partial \zeta^2} + \frac{\partial^2}{\partial x^{*2}}\right)\hat{w}^*, \tag{5.10d}$$

where

$$U^* = U\cos\beta + E^{-1}\,V\sin\beta \tag{5.10e}$$

and

$$V^* = -U\sin\beta + E^{-1}\,V\cos\beta \tag{5.10f}$$

are the mean velocity components in the x^* and y^* directions, respectively. We can now define a stream function from (5.10a) by

$$\hat{u}^* = \partial\psi/\partial\zeta, \quad \hat{w} = -\partial\psi/\partial x^*, \tag{5.11}$$

and take a perturbation of the form

$$\psi = \phi(\zeta)\,e^{i\alpha(x^*-ct)}, \quad \hat{v}^* = \theta(\zeta)\,e^{i\alpha(x^*-ct)}, \tag{5.12a,b}$$

and

$$\hat{P} = \pi(\zeta)\,e^{i\alpha(x^*-ct)}. \tag{5.12c}$$

Upon substitution and elimination of the pressure from (5.10b) and (5.10d), we obtain

$$i\alpha(U^*-c)(\phi''-\alpha^2\phi) - i\alpha U^{*\prime\prime}\phi - \frac{2}{E\,Re}\theta' = \frac{1}{Re}(\phi^{\mathrm{IV}} - 2\alpha^2\phi'' + \alpha^4\phi), \tag{5.13}$$

while (5.10c) yields

$$i\alpha(U^*-c)\,\theta - i\alpha V^{*\prime}\phi + \frac{2}{E\,Re}\phi' = \frac{1}{Re}(\theta'' - \alpha^2\theta), \tag{5.14}$$

where a prime denotes $d/d\zeta$. As the Rossby number ($E\,Re$) tends to infinity (5.13) becomes the Orr–Sommerfeld equation, whose solution could then be used to determine $\theta(\zeta)$ from (5.14). In general, the equations are coupled.

In order to obtain a solution we take advantage of the fact that the experimentally observed wavenumbers are small, and expand in terms of α in a manner identical to that used by Yih (1963) for the inclined-plane flow (also Yih 1965, pp. 180–189). Actually, such an expansion also requires that $\alpha\,Re$ be small, and, from figure 9, we see that the condition is met only at the larger values of the radius for a fixed flow rate. However, from the inclined-plane analysis we might expect the qualitative trends to be significant. We then assume that E is large and also expand in inverse powers of E. Hence, we expand ϕ, θ and c in double expansions of the form

$$\phi = \sum_{i,j=0} \alpha^i E^{-j}\phi_{ij}, \tag{5.15}$$

but carry the details through only for $i = j = 1$. With reference to (5.10e,f), we also write

$$U^* = U_0^* + E^{-1}U_1^* + \ldots, \quad V^* = V_0^* + E^{-1}\,V_1^* + \ldots, \tag{5.16}$$

where the definitions of the U_j^*, V_j^* are obvious. The following equations are then obtained.

$$O(\alpha^0 E^0)\colon \phi_{00}^{\mathrm{IV}} = 0, \theta_{00}'' = 0. \tag{5.17a,b}$$

$$O(\alpha^0 E^{-1})\colon \phi_{01}^{\mathrm{IV}} = -2\theta_{00}', \theta_{01}'' = 2\phi_{00}'. \tag{5.18a,b}$$

$$O(\alpha^1 E^0)\colon \phi_{10}^{\mathrm{IV}} = iRe[(U_0^* - c_{00})\phi_{00}'' - U_0^{*\prime\prime}\phi_{00}], \tag{5.19a}$$

$$\theta_{10}'' = iRe\,[(U_0^* - c_{00})\theta_{00} - V_0^{*\prime}\phi_{00}]. \tag{5.19b}$$

$$O(\alpha^1 E^{-1})\colon \phi_{11}^{\mathrm{IV}} = iRe[(U_0^* - c_{00})\phi_{01}'' - U_0^{*\prime\prime}\phi_{01} + (U_1^* - c_{01})\phi_{00}'' - U_1^{*\prime\prime}\phi_{00}] - 2\theta_{10}', \tag{5.20a}$$

$$\theta_{11}'' = iRe\,[(U_0^* - c_{00})\theta_{01} - V_0^{*\prime}\phi_{01} + (U_1^* - c_{01})\phi_{00} - V_1^{*\prime}\phi_{00}] + 2\phi_{10}'. \tag{5.20b}$$

The above equations are to be solved subject to the condition of no slip at the wall, i.e.

$$\phi_{ij}(1) = \phi_{ij}'(1) = \theta_{ij}(1) = 0, \tag{5.21}$$

and also subject to the free-surface stress conditions, which will now be formulated. We need to know the wave-induced displacement, $\epsilon\delta\hat{\eta}$ say, of the free surface, which is determined by

$$\frac{\partial\hat{\eta}}{\partial t} + U^*(0)\frac{\partial\hat{\eta}}{\partial x^*} = \hat{w}(x^*, 0, t) \tag{5.22a}$$

or, if we let $\hat{\eta} = \eta \exp\{i\alpha(x^* - ct)\}$,

$$\eta = -\phi(0)/(U^*(0) - c). \tag{5.22b}$$

The shear stress must vanish at the free surface, so

$$\frac{\partial v^*}{\partial\zeta} = \frac{\partial u^*}{\partial\zeta} + \frac{\partial w}{\partial x} = 0 \quad \text{at} \quad \zeta = \hat{n}. \tag{5.23}$$

Expanding about the mean level, we obtain

$$\frac{d\theta}{d\zeta} + \eta\frac{d^2V^*}{d\zeta^2} = 0 \tag{5.24}$$

and

$$\frac{d^2\phi}{d\zeta^2} + \alpha^2\phi + \eta\frac{d^2U^*}{d\zeta^2} = 0, \tag{5.25}$$

to be applied now at $\zeta = 0$. Using (5.22*b*) and (5.15), we obtain from (5.24)

$$(U_0^* - c_{00})\frac{d\theta_{00}}{d\zeta} - \phi_{00}\frac{d^2V_0^*}{d\zeta^2} = 0, \tag{5.24a}$$

$$(U_0^* - c_{00})\frac{d\theta_{01}}{d\zeta} + (U_1^* - c_{01})\frac{d\theta_{00}}{d\zeta} - \phi_{01}\frac{d^2V_0^*}{d\zeta^2} - \phi_{00}\frac{d^2V_1^*}{d\zeta^2} = 0, \tag{5.24b}$$

$$(U_0^* - c_{00})\frac{d\theta_{10}}{d\zeta} - c_{10}\frac{d\theta_{00}}{d\zeta} - \phi_{10}\frac{d^2V_0^*}{d\zeta^2} = 0, \tag{5.24c}$$

and

$$(U_0^* - c_{00})\frac{d\theta_{11}}{d\zeta} + (U_1^* - c_{01})\frac{d\theta_{10}}{d\zeta} - c_{10}\frac{d\theta_{01}}{d\zeta} - c_{11}\frac{d\theta_{00}}{d\zeta} - \frac{d^2V_0^*}{d\zeta^2}\phi_{11} - \frac{d^2V_1^*}{d\zeta^2}\phi_{10} = 0, \tag{5.24d}$$

whereas, from (5.25) we have

$$(U_0^*-c_{00})\frac{d^2\phi_{00}}{d\zeta^2}-\frac{d^2U_0^*}{d\zeta^2}\phi_{00}=0, \tag{5.25a}$$

$$(U_0^*-c_{00})\frac{d^2\phi_{01}}{d\zeta^2}+(U_1^*-c_{01})\frac{d^2\phi_{00}}{d\zeta^2}-\frac{d^2U_0^*}{d\zeta^2}\phi_{01}-\frac{d^2U_1^*}{d\zeta^2}\phi_{00}=0, \tag{5.25b}$$

$$(U_0^*-c_{00})\frac{d^2\phi_{10}}{d\zeta^2}-c_{10}\frac{d^2\phi_{00}}{d\zeta^2}-\frac{d^2U_0^*}{d\zeta^2}\phi_{10}=0, \tag{5.25c}$$

$$(U_0^*-c_{00})\frac{d^2\phi_{11}}{d\zeta^2}+(U_1^*-c_{01})\frac{d^2\phi_{10}}{d\zeta^2}-c_{10}\frac{d^2\phi_{01}}{d\zeta^2}$$
$$-c_{11}\frac{d^2\phi_{00}}{d\zeta^2}-\frac{d^2U_0^*}{d\zeta^2}\phi_{11}-\frac{d^2U_1^*}{d\zeta^2}\phi_{10}=0. \tag{5.25d}$$

By again expanding about $\zeta=0$, the normal stress condition can be written as

$$-\frac{\hat{\eta}}{F^2}-\hat{p}+\frac{2}{Re}\frac{\partial\hat{w}}{\partial\zeta}+We\frac{\partial^2\hat{\eta}}{\partial x^2}=0 \tag{5.26}$$

at $\zeta=0$, where We is the Weber number, or

$$\frac{\eta}{F^2}+\bar{\pi}+\frac{2i\alpha}{Re}\frac{d\phi}{d\zeta}+\alpha^2\,We\,\eta=0. \tag{5.27}$$

From the x^* momentum equation, we find $\bar{\pi}$ to be

$$\bar{\pi}=-(U^*-c)\frac{d\phi}{d\zeta}+\frac{dU^*}{d\zeta}\phi-\frac{2i}{\alpha\,Re\,E}\theta-\frac{i}{\alpha\,Re}\left(\frac{d^3\phi}{d\zeta^3}-\alpha^2\frac{d\phi}{d\zeta}\right). \tag{5.28}$$

After substituting for $\bar{\pi}$ and expanding in terms of E^{-1} and α, we have from (5.27)

$$d^3\phi_{00}/d\zeta^3=0, \tag{5.27a}$$

$$d^3\phi_{01}/d\zeta^3=-2\theta_{00}, \tag{5.27b}$$

$$\frac{d^3\phi_{10}}{d\zeta^3}=i\,Re\left[(U_0^*-c_{00})\frac{d\phi_{00}}{d\zeta}-\frac{dU_0^*}{d\zeta}\phi_{00}\right]+i\,Re\left(\alpha^2\,We+\frac{1}{F^2}\right)\left(\frac{\phi_{00}}{U_0^*-c_{00}}\right), \tag{5.27c}$$

$$\frac{d^3\phi_{11}}{d\zeta^3}=-2\theta_{10}+iRe\left[(U_0^*-c_{00})\frac{d\phi_{01}}{d\zeta}-\frac{dU_0^*}{d\zeta}\phi_{01}+(U_1^*-c_{01})\frac{d\phi_{00}}{d\zeta}-\frac{dU_1^*}{d\zeta}\phi_{00}\right]$$
$$+i\,Re\left(\frac{1}{F^2}+\alpha^2\,We\right)\left[\frac{\phi_{01}}{U_0^*-c_{00}}-\frac{\phi_{00}}{U_0^*-c_{00}}\left(\frac{U_1^*-c_{01}}{U_0^*-c_{00}}\right)\right]. \tag{5.27d}$$

The term $\alpha^2\,We$ is included, as in the inclined-plane analysis, on the basis that the Weber number can be quite large for common fluids and some flow conditions.

The solution
$$\phi_{00}=(1-\zeta)^2 \tag{5.29}$$
satisfies (5.17*a*), (5.21), and (5.22*a*), and c_{00} is then determined from (5.25*a*) as

$$c_{00}=3\cos\beta. \tag{5.30}$$

From (5.17*b*), (5.21) and (5.24*a*), we also find

$$\theta_{00}=2(1-\zeta)\tan\beta. \tag{5.31}$$

The case $\beta \to \frac{1}{2}\pi$ will be discussed briefly below. At $O(E^{-1})$, the solution

$$\phi_{01} = \tfrac{1}{3}\tan\beta\{-\zeta+\tfrac{5}{2}\zeta^2-2\zeta^3+\tfrac{1}{2}\zeta^4\} \tag{5.32}$$

satisfies (5.18a) (5.21) and (5.27b); it also satisfies (5.25b) if

$$c_{01} = -4\sin\beta. \tag{5.33}$$

(In writing (5.32) we have deleted any multiple of the homogeneous solution.) Hence, the wave speed is unaffected for waves which travel in the x direction. Oblique waves, however, can actually have a greater wave speed to this order for sufficiently small negative β. To complete the solution, we have

$$\theta_{01} = \tfrac{10}{3}+\tfrac{11}{3}\tan^2\beta-(2+\tfrac{11}{3}\tan^2\beta)\,\zeta-2\zeta^2+\tfrac{2}{3}\zeta^3, \tag{5.34}$$

a solution which satisfies (5.18b), (5.21) and (5.24b).

The $O(\alpha)$ problem is identical to that for an oblique disturbance in the inclined-plane flow. The solution

$$\phi_{10} = J_{10}\zeta+K_{10}\zeta^2+L_{10}\zeta^3-\tfrac{1}{20}i\,Re\cos\theta\zeta^5, \tag{5.35}$$

where

$$L_{10} = i\,Re\left[\tfrac{1}{2}\cos\beta-\frac{1}{9\cos\beta}\left(\alpha^2\,We+\frac{1}{F^2}\right)\right], \tag{5.35a}$$

$$K_{10} = -2c_{10}/3\cos\beta, \quad J_{10} = \tfrac{1}{20}i\,Re\cos\beta-K_{10}-L_{10}, \tag{5.35b,c}$$

satisfies (5.19c), (5.25c) and (5.27c) and the first part of (5.21). It also satisfies the second part of (5.21) if

$$c_{10} = i\,Re\,[\tfrac{6}{5}\cos^2\beta-\tfrac{1}{3}(\alpha^2\,We+1/F^2)]. \tag{5.36}$$

As one might expect, this result states that the growth rate is a maximum for waves which travel in the direction of the lowest order mean flow ($\beta = 0$). Hence, for fixed flow conditions the waves on the disk should appear to be almost concentric at the *larger* values of the radius. The solution at the next order will indicate how this conclusion might be modified for finite Ekman numbers. To complete the solution at this order, we find

$$\theta_{10} = \tfrac{5}{4}i\,Re\sin\beta+\frac{4c_{10}\tan\beta}{3\cos\beta}(\zeta-1)-\tfrac{3}{2}i\,Re\sin\beta\,(\zeta^2-\tfrac{1}{6}\zeta^4), \tag{5.37}$$

which satisfies (5.19b), (5.21) and (5.24c).

Finally, at $O(\alpha E^{-1})$, we obtain

$$\phi_{11} = J_{11}\zeta+K_{11}\zeta^2+L_{11}\zeta^3-\frac{c_{10}\tan\beta}{9\cos\beta}\zeta^4+i\,Re\sin\beta\left[\frac{17}{5!}\zeta^5-\frac{1}{210}\zeta^7\right], \tag{5.38}$$

where

$$L_{11} = \frac{4c_{10}\tan\beta}{9\cos\beta}-i\,Re\left(\alpha^2\,We+\frac{1}{F^2}\right)\left(\frac{11\tan\beta}{54\cos\beta}\right)-\tfrac{5}{4}i\,Re\sin\beta, \tag{5.38a}$$

$$K_{11} = -\frac{16}{9}\frac{c_{10}\tan\beta}{\cos\beta}-\frac{2c_{11}}{3\cos\beta}, \tag{5.38b}$$

$$J_{11} = -i\,Re\sin\beta\left(\frac{17}{120}-\frac{1}{210}\right)+\frac{c_{10}\tan\beta}{9\cos\beta}-K_{11}-L_{11}. \tag{5.38c}$$

This solution satisfies (5.20*a*) (5.25*d*) and (5.27*d*), and the first part of (5.21); it satisfies the second part of (5.21) if

$$c_{11} = \tfrac{1}{2}(i\,Re\sin 2\beta)\,[\tfrac{17}{16} - \tfrac{1}{20} - \tfrac{17}{80} + \tfrac{1}{140} - \tfrac{22}{10} - \tfrac{15}{4}]$$
$$= -2{\cdot}571\,i\,Re\sin 2\beta. \tag{5.39}$$

Hence, to the order considered, we have

$$c = 3\cos\beta - 4E^{-1}\sin\beta + i\alpha Re\,[\tfrac{6}{5}\cos^2\beta - \tfrac{1}{3}(\alpha^2 We + 1/F^2) - 2{\cdot}571E^{-1}\sin 2\beta]. \tag{5.40}$$

Although the growth rate is always less for $\beta > 0$ than for $\beta = 0$, the converse can hold for $\beta < 0$. In fact, the terms in brackets which are dependent upon β have a maximum for

$$\tan 2\beta = -4{\cdot}28E^{-1}. \tag{5.41}$$

For the values $E^{-1} = 0{\cdot}05$, $0{\cdot}1$ and $0{\cdot}5$, corresponding values of β for maximum c_i are $-6°$, $-11{\cdot}6°$ and $-32{\cdot}5°$, respectively. Negative values of β would correspond to spirals which open in the direction of rotation, as observed, and the given values of β are in reasonable agreement (cf. figure 9) with the observed values (if the spatial growth rate were maximized, the sign of β would remain unchanged, but $\tan\beta$ would no longer be only a function of E but a complicated function of E, α, We and F^2). On the other hand, the wave speed is increased somewhat relative to the case $\beta = 0$, which is not in agreement with the observed spiral waves.

Some of the results given, e.g. θ_{00} in (5.31), appear to become singular as $\beta \to \frac{1}{2}\pi$. This occurs because our expansion is restricted to cases when $U^*(0) - c$ is of order unity, as can be seen from the kinematic condition for the surface deflexion (5.22*b*). For $\beta \to \frac{1}{2}\pi$, this term is $O(E^{-1})$ or $O(\alpha\,Re)$, depending upon the magnitude of $\alpha\,Re\,E$. When $\alpha\,Re\,E \ll 1$, so that $c \sim O(E^{-1})$, we must rescale the expansion so that $\phi \sim O(E^{-1})$ in order to have $\eta \sim O(1)$, while θ remains of order unity, as can be seen from the shear stress condition (5.24). When $(\alpha\,Re\,E) \gg 1$, so that $c \sim O(\alpha)$, then $\phi \sim O(\alpha)$ and $\theta \sim O(1)$. In either case, the fact that the eigenvalue relation is not singular indicates that the result for c is valid for arbitrary β, which can easily be shown to be true for the latter case. For the former case, from (5.40), the analysis should be valid provided that $(4/3E)\tan\beta \ll 1$, a condition which is met by much of the experimental data.

The Coriolis force is manifested in two ways in the present problem, namely, in creating a mean flow component normal to the direction of the body force, whose effect can be felt via the convective terms and the boundary conditions, and in directly affecting the disturbance via the $(\boldsymbol{\omega} \times \hat{\mathbf{u}})$ terms in the linearized stability equations. In order to assess the importance of the latter effect, terms representing it were dropped from the analysis, so that the problem reduced to that of the stability of a flow with two spatially varying velocity components in a non-rotating system. The result for c was found to be

$$c = 3\cos\beta - \tfrac{11}{4}E^{-1}\sin\beta + i\alpha\,Re\,[\tfrac{6}{5}\cos^2\beta - \tfrac{1}{3}(\alpha^2\,We + 1/F^2) - 4{\cdot}94\,E^{-1}\sin 2\beta]. \tag{5.42}$$

By comparing this result with (5.40), we see that the direct effect of the Coriolis force upon the disturbance is to decrease the angle of maximum

growth for a given value of E. It can also be shown that the maximum growth rate is decreased.

Assuming the asymptotic mean flow solution to be valid, it is difficult to see what mechanism might give rise to the stationary pattern. The inflexion-point type of instability, which has been discussed by Gregory, Stuart & Walker (1955) and is appropriate for boundary-layer instability in rotating flows at large values of the Reynolds numbers, would occur only for positive values of β, and β large so that $\tan\beta \sim E$. One mechanism of instability which has been omitted on the basis of the parallel-flow model is the effect of centripetal acceleration upon the curved free surface. Here, we have in mind the type of instability discussed by Yih (1960) for a film on the surface of a rotating cylinder. However, this effect would be felt by the departure of the pressure distribution from the hydrostatic variation and, from the asymptotic solution, would lead to a modification of the Froude number term in the normal stress condition (5.26) by a term of $O(\delta\omega^2/g)$, which would appear to be small. Hence, we can only conclude that the characteristics of the spiral wave are somehow fixed in a region in which the asymptotic solution is completely invalid. A more refined stability analysis, using the rotating-disk geometry, would need to consider the relative magnitudes of E^{-2} and $(ER_0)^{-1}$. Terms of the former type emphasize the departure of the mean flow parallel to the disk from the radial direction and the effect of the Coriolis force upon the disturbance (which is very important in the Ekman layer stability problem; cf. Lilly (1966)). Terms of the latter type reflect the effects of the mean vertical velocity and surface curvature (which would bring in new terms involving the surface tension) and, as shown by Rauscher (1969), the error involved in assuming a local stability analysis to be valid. The effects of the air upon both the mean and perturbed motions should also be assessed more carefully. For instance, Craik (1966) has shown that the tangential stress perturbation at the interface can play an important role in the study of wind-generated waves in very thin liquid films.

6. Film breakup

The breakup of the film is illustrated in figure 15 (plate 3). It shows a series of frames taken during an uninterrupted test during which the flow rate was varied continuously at constant rotational speed. Typically, as the film thins out one begins to see 'incipient' dry spots (figure 15(*a*)). These appear to be disturbances on the film surface caused by dust particles which have settled on the disk. Finally, the film breaks usually, but not necessarily, immediately downstream of these protruberances and the number of these dry spots increases. (Ultimately, the film breaks up entirely and flows in 'rivulets'.) The film breakup exhibits a pronounced 'hysteresis.' Dry spots can be destroyed by wiping the disk; they will reappear spontaneously when the film is sufficiently thin.

When the film is relatively thick the dry spots are fairly irregular and have a blunt leading edge (cf. 'dry patches' on plane films flowing under gravity). When the film is thin and the rotational speed is high, they exhibit sharp leading edges and a very regular triangular shape. The fluid 'accumulates' along the

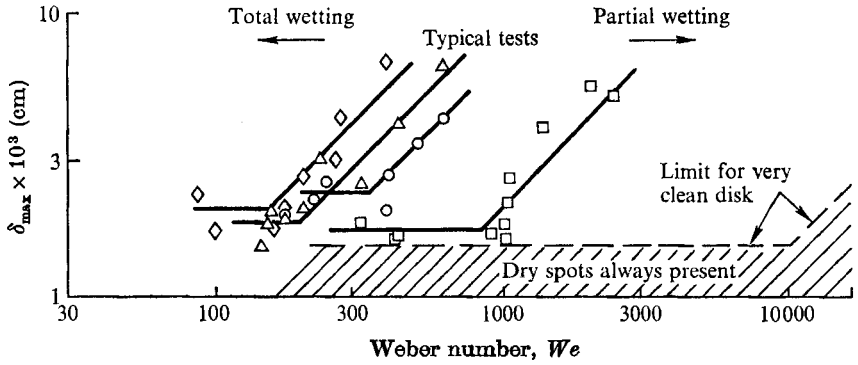

FIGURE 16. Conditions for the occurrence of dry spots. □, $Q = 1{\cdot}0$ c.c./s; ○, $Q = 1{\cdot}67$ c.c./s; △, $Q = 2{\cdot}5$ c.c./s; ◇, $Q = 3{\cdot}33$ c.c./s; $\nu^* = \sigma^* = 1$; δ_{max} is the film thickness at which dry spots first appear.

edges of the triangle; it appears that the film thickness between spots is not affected (see also the oscilloscope trace, figure 6). The wave motion does not seem to influence the breakdown of the film; waves appear at the same flow condition whether dry spots are present or not.

It is quite difficult to correlate these observations in a quantitative way because they depend so much on the cleanliness of the disk (wetting properties) and exhibit such a pronounced hysteresis. The following is intended to be a practical guide for the experimenter rather than a scientific study of the phenomenon. The observations we shall discuss are based on tests in which flow conditions were fixed, dry spots were 'wiped off' and then observed as they reappeared spontaneously in a period of the order of ten seconds.

It seems that two distinct mechanisms are operative; these are evident on figure 16. When the film becomes sufficiently thin (below 20 μm) the breakdown is caused by particles (incipient dry spots), probably dust, which are entrained by the fluid and stick to the surface of the disk. The appearance of dry spots is then dependent only on the film thickness and is thus independent of surface tension. Dry spots are distributed randomly around the circumference of the disk and their number increases with radius. The value of the film thickness shown on figure 16 (δ_{max}) corresponds to the place on the disk where these dry spots first appear. When the film is thicker breakdown occurs 'naturally', that is, without visible disturbance, as a function of the flow parameters, specifically, the Weber number. Figure 16 shows this for a typical experiment. The intercept on this logarithmic plot of the film thickness at which dry spots appear against the local Weber number is roughly proportional to Q^2. The figure also indicates a limit below which, in this particular experimental situation (wetting properties), which is fairly typical of laboratory practice, one can always expect dry spots to occur.

7. Concluding remarks

The results of the present experiment define fairly completely the flow of a thin liquid film on a rotating disk and the condition of the free surface. The use of surface-active agents to vary the apparent surface tension deserves further theoretical and experimental attention, particularly in view of the strong influence of this parameter on the stability of the film. In practical terms, the results allow one to select design parameters such that the film surface will be smooth or wavy. One can expect that the interphase heat- or mass-transfer coefficients will vary considerably between these two conditions, which is an important consideration in most applications of thin-film flows.

The present research was sponsored by the Department of Health, Education and Welfare, National Institute of Health, Grant He 11763. The authors wish to acknowledge the substantial contributions made by Mr A. Campfield and Mr J. Rausher, graduate research assistants, to various phases of this work.

REFERENCES

AROESTY, J., GROSS, J. F., ILLICKAL, M. M. & MALONEY, J. V. 1967 Blood oxygenation: a study in bioengineering Mass transfer. *Digest Seventh Int. Conf. on Medical and Biological Engineering, Stockholm*, p. 527. (See also, 1967 *RAND Corporation, Rep.* P-8732.)

BENJAMIN, T. B. 1957 Wave formation in laminar flow down an inclined plane. *J. Fluid Mech.* **2**, 554–574.

BENJAMIN, T. B. 1964 Effects of surface contamination on wave formation in falling liquid films. *Arch. Mech. Stos.* **16**, 615–626.

BINNIE, A. M. 1957 Experiments on the onset of wave formation on a film of water flowing down an inclined plane. *J. Fluid Mech.* **2**, 551–553.

BROMLEY, L. A. 1965 Saline water conservation research. *Water Resources Center, University of California, San Diego Contribution*, no. 100, 24–30.

CHARWAT, A. F., KELLY, R. E., GAZLEY, C. & CAMPFIELD, L. A. 1970 The development and the stability of thin liquid films on a rotating disk. *U.C.L.A. Tech. Rep.* ENG-7047.

CRAIK, A. D. D. 1966 Wind-generated waves in thin liquid films. *J. Fluid Mech.* **26**, 369–392.

DORFMAN, L. A. 1967 Heat transfer and viscous liquid flow on a rotating disk. *J. Engng. Phys.* **12**, 309–316.

ESPIG, H. & HOYLE, R. 1965 Waves in a thin liquid layer on a rotating disk. *J. Fluid Mech.* **22**, 671–677

FULFORD, G. D. 1964 The flow of liquids in thin films. *Advances in Chem. Eng.* **5**, 151–263.

GAZLEY, C. & CHARWAT, A. F. 1968 The characteristics of thin liquid films on a spinning disk. *Proc. Third All-Union Conference on Heat and Mass Transfer, Minsk.* (See also, 1968 *RAND Corporation. Rep.* P-3851.)

GREGORY, N., STUART, J. T. & WALKER, W. S. 1955 On the stability of three-dimensional boundary layers with application to the flow due to a rotating disk. *Phil. Trans. Roy. Soc.* A **248**, 155–199.

LILLY, D. K. 1966 On the instability of Ekman boundary flow. *J. Atmos. Sci.* **23**, 481–494.

RAUSCHER, J. W. 1969 Stability of a liquid film on a spinning disk. *U.C.L.A. School of Engineering and Applied Science Rep.* no. 69–44. (See also 1969 M.S. thesis, U.C.L.A.)

RAUSCHER, J. W., KELLY, R. E. & COLE, J. D. 1972 An asymptotic solution for laminar flow of a thin film on rotating disk. *J. Appl. Mech.* (to be published).

SCHLICHTING, H. 1960 *Boundary Layer Theory*, 4th edn. McGraw-Hill.

TAILBY, S. R. & PORTALSKI, S. 1962 The determination of the wavelength on a vertical film of liquid flowing down a hydrodynamically smooth plate. *Trans. Inst. Chem. Eng.* **40**, 114–121.

WHITAKER, S. 1964 Effect of surface active agents on the stability of falling liquid films. *Indust. & Engng. Chem. Fund.* **3**, 132–142.

YIH, C.-S. 1960 Instability of a rotating film with a free surface. *Proc. Roy. Soc.* A **258**, 63–81.

YIH, C.-S. 1963 Stability of liquid flow down an inclined plane. *Phys. Fluids*, **6**, 321–334.

YIH, C.-S. 1965 *Dynamics of Nonhomogeneous Fluids*. Macmillan.

FIGURE 4. Examples of waves occurring on the surface of the disk

	Q(c.c./s)	ω'(rev/s)	σ^*	ν^*
(*a*) Smooth film	5	1	0·95	1·0
(*c*) Spiral waves	2·5	6	0·98	1·7

	Q(c.c./s)	ω'(rev/s)	σ^*	ν^*
(*b*) Concentric waves	12	1	0·95	1·0
(*d*) Irregular break up of spiral waves	10·8	10	0·96	1·0

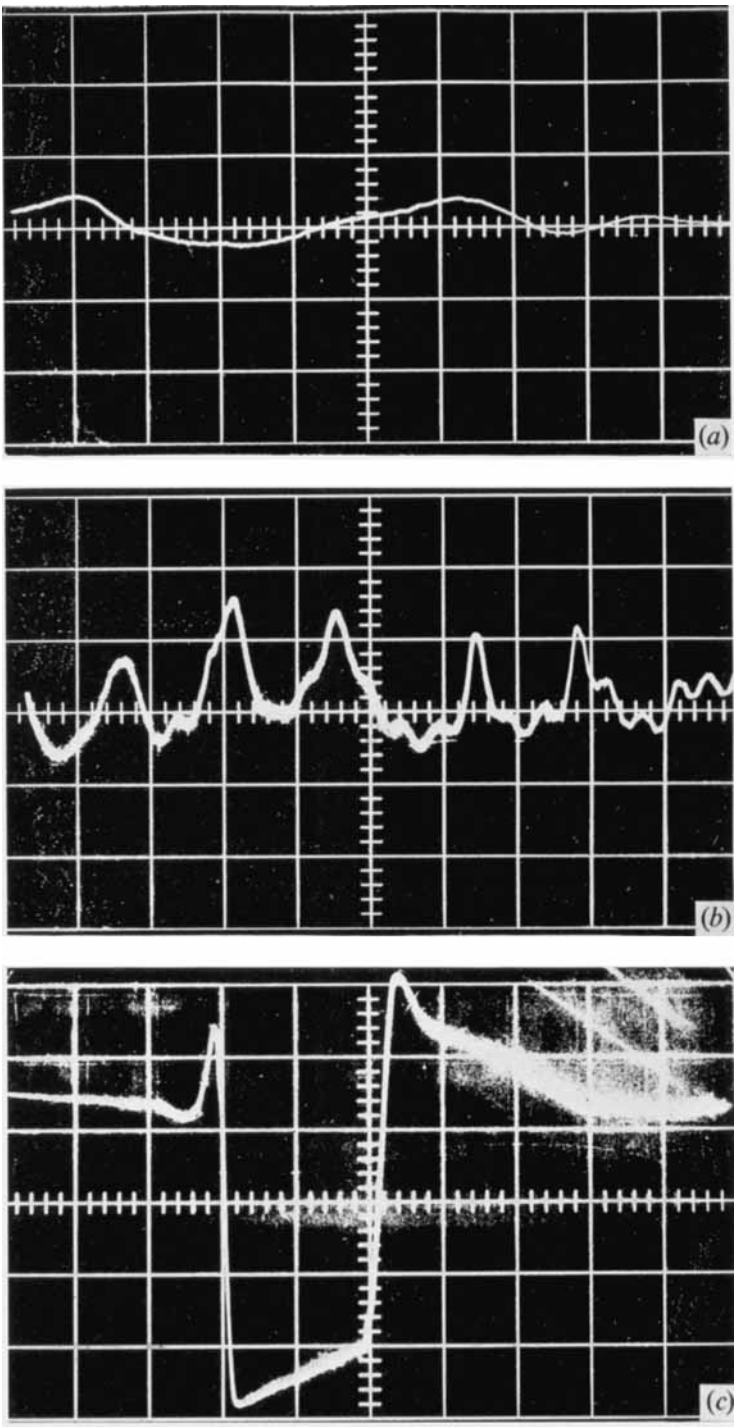

FIGURE 6. Oscilloscope traces of wave patterns, $r = 5$ cm. (*a*) Concentric wave, $Q = 11{\cdot}6$ c.c./s, $\omega' = 1$ rev/s. (*b*) Spiral wave, $Q = 3{\cdot}34$ c.c./s, $\omega' = 6$ rev/s. (*c*) Dry spot, $Q = 2{\cdot}5$ c.c./s, $\omega' = 3$ rev/s.

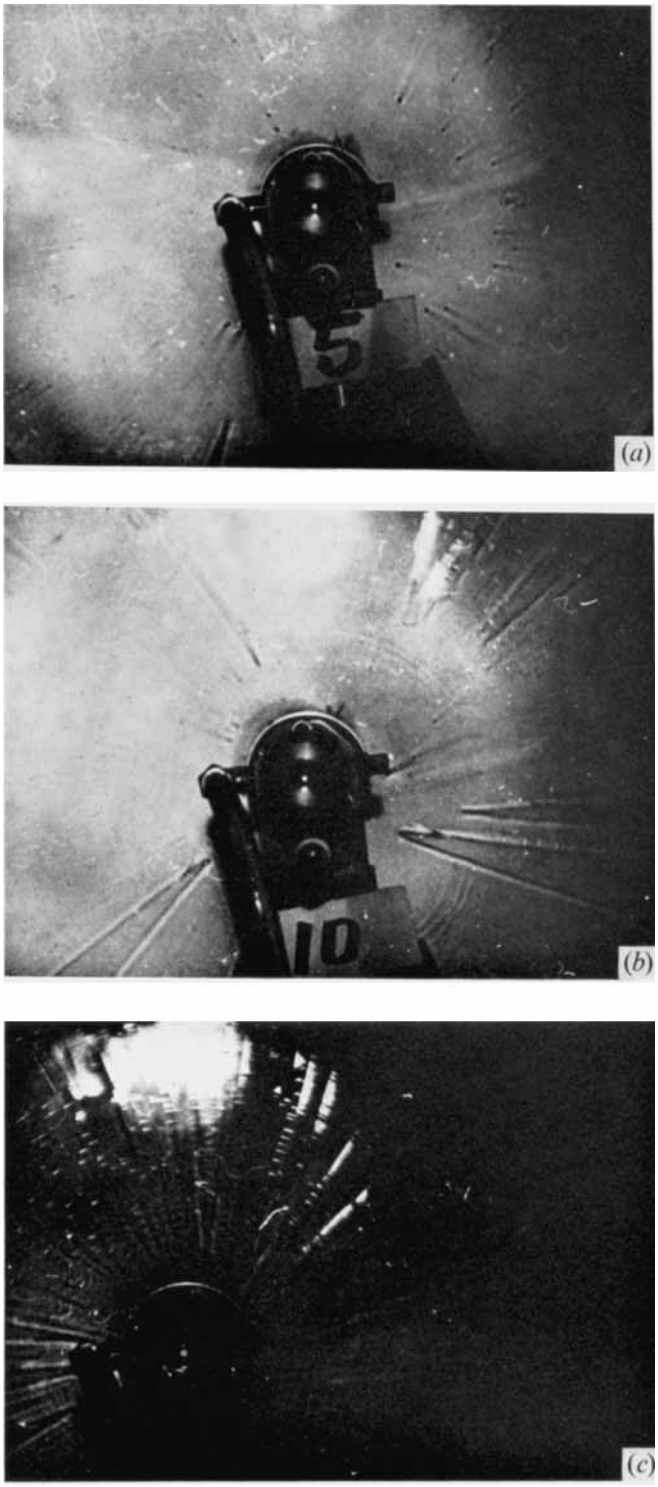

FIGURE 15. Examples of dry spots at high rotational speeds. $Q = 100$ c.c./min, $\nu' = 1{\cdot}7$, $\sigma^* = 0{\cdot}98$. Direction of rotation is clockwise. (*a*) $\omega' = 4$ rev/s, (*b*) $\omega' = 6$ rev/s, (*c*) $\omega' = 9$ rev/s.